metals

MDPI

Article

The Effect of Creep Aging on the Fatigue Fracture Behavior of 2524 Aluminum Alloy

Wenke Li [1], Lihua Zhan [1,2,*], Lingfeng Liu [1] and Yongqian Xu [1]

[1] Light Metal Research Institute, Central South University, Changsha 410083, China; lwk1992@csu.edu.cn (W.L.); goodlucky321@yeah.net (L.L.); 143812027@csu.edu.cn (Y.X.)

[2] National Key Laboratory of High Performance Complex Manufacturing, Central South University, Changsha 410083, China

* Correspondence: yjs-cast@csu.edu.cn; Tel.: +86-731-88830254

Academic Editor: Nong Gao

Received: 26 July 2016; Accepted: 31 August 2016; Published: 7 September 2016

Abstract: Normal temperature tensile and fatigue tests were adopted to test the mechanical performance and fatigue life of 2524 aluminum alloy under the three states of T3, artificial aging, and creep aging, and scanning electron microscope and transmission electron microscope were also used to observe the fatigue fracture morphology and aging precipitation features of the alloy under the above three states. Results showed that the alloy treated by creep aging can obtain higher fatigue life, but that treated by artificial aging is lower than T3; T3 alloy is mainly dominated by GPB region. Meanwhile, the crystal boundary displays continuously distributed fine precipitated phases; after artificial aging and creep aging treatment, a large amount of needle-shaped S′ phases precipitate inside the alloy, while there are wide precipitated phases at the crystal boundary. Wide precipitation free zones appear at the crystal boundary of artificial-aging samples, but precipitation free zones at the alloy crystal boundary of creep aging become narrower and even disappear. It can be seen that creep aging can change the precipitation features of the alloy and improve its fatigue life.

Keywords: 2524 aluminum alloy; creep aging; fatigue fracture behavior; aging precipitation

1. Introduction

Creep aging forming, as a processing method that utilizes the creep deformation of metal and the aging features enhancement of aluminum alloy, has been mainly applied to manufacturing plane wallboard and other whole-piece wallboard members [1,2]. Compared with conventional plastic forming, creep aging enjoys high forming accuracy and repeatibility, hence reducing the risk of materials cracking in processing and residual stress of components [3,4]. Therefore, scholars have conducted in-depth research on the resilience prediction and performance of creep aging forming. Zhan et al. [5] built a constitutive model that could simulate the change rules of the strain changes of creep aging, precipitated phase changes, dislocation strengthening, solution strengthening, aging strengthening, and material property in the process of forming by combining uni-directional tensile tests. Hargarter et al. [6] studied the influence of a precipitated phase position under stress upon the yield strength of Al-Cu-Mg-Ag and Al-Cu alloys, discovering that the yield strength of materials of stress aging was lower than that of non-stress under the same heat treatment condition. Li et al. [7] studied the influence of different aging forming parameters (aging time, temperature) upon the organizational property of 2124 aluminum alloy and pointed out that the presence of stress accelerated the precipitation and transition of the strengthening phases of 2124 aluminum alloy. Chen et al. [8] explored the creep aging behaviors of 7050 aluminum alloy under a solution hardening state and pre-treatment state and discovered that, after pre-deformation, creep aging deformation of the material became larger. Higher temperature and stress led to greater creep aging deformation.

However, the service environment of modern aviation equipment has been expanding rapidly. Thus, apart from the requirements for material strength and toughness, sound service performance is also demanded, especially fatigue life. Therefore, there has been much research on the fatigue performance of aviation materials. Zabett et al. [9] studied the influence of micro organization upon production and expansion behaviors of the cracks of 2024-T351 in three directions and found out that cracks mainly appeared at a secondary phase fracture of Al_7Cu_2Fe and crack production would reduce fatigue life of the alloy. Carte et al. [10] explored the fatigue crack expansion performance of 7475 aluminum alloy and concluded that, with the increase of crystal particle size, the fatigue crack expansion speed dropped. Bray et al. [11] studied the influence of aging treatment upon the fatigue crack expansion speed of 2024 aluminum alloy and discovered that high-density solution clusters at the beginning of aging improved alloy fatigue performance.

To date, there has been much research on creep aging forming and aviation materials performance test, but few have involved materials performance after creep aging, especially service performance. 2524-T3 aluminum alloy, as a new type of highly strong Al-Cu-Mg aluminum alloy developed after 2024 and 2124 aluminum alloys [12], has been applied to Boeing 777 and Airbus A380 [13]. Therefore, this paper regards 2524 aluminum alloy as a research object and compares its micro structure, mechanical property, and fatigue performance after artificial aging and creep aging, so as to provide an experimental foundation for a creep aging forming technique of 2524 aluminum alloy.

2. Materials and Methods

The material used in this experiment was provided by Southwest Aluminum (Group) Co., Ltd., (Chongqing, China), namely 2.5-mm 2524-T3 aluminum alloy, whose chemical components (wt. %) include 4.26Cu-1.36Mg-0.57Mn-0.037Fe-0.024Zn-0.01Ti-0.002Cr-0.089Si-(bal.)Al. The heat treatment state of T3 refers to cold processing after solution treatment followed by natural aging to a basically stable state. First, hardness samples were taken for artificial aging under 180 °C and a hardness test under a Huayin microscopic hardness meter (Huayin Testing Instrument Co., Ltd., Yantai, China), so as to obtain an aging hardening curve; by analyzing the curve, it was obtained that the time for reaching peak aging was 12 h. Then, conventional artificial aging treatment and creep aging treatment were conducted on a plate, for which a RWS50 electron creep slackness tester (Changchun Research Institute for Machanical Science Co., Ltd., Changchun, China) was adopted for creep aging (CA: 180 °C × 180 MPa × 12 h), while airing dryer machine was used for artificial aging (AA: 180 °C × 12 h).

A room temperature tensile performance test and fatigue life test were conducted on the alloys at the three states, namely, the 2524-T3 state, after artificial aging, and after creep aging. Both of the tests were conducted on the MTS810 tester machine (MTS Systems Corporation, Eden Prairie, MN, USA). There were three horizontal tests of mechanical performance, with a tensile speed of 2 mm/min. Sine wave loading was adopted for the fatigue life test samples, with a frequency of 10 Hz and stress ratio of 0.1 (30/300 MPa). For each state, five horizontal samples were taken.

Fatigue sample fracture was captured to be observed under a TESCAN scanning electron microscope (Tescan company, Brno, Czech), so as to study the production and expansion of cracks. Micro organizations were observed under TecnaiG220 transmission electron microscope (United States FEI limited liability company, Hillsboro, OR, USA). Samples were thinned to 0.08 mm first and then thinned again on a TenuPol-5 electrolyzation double spraying thinner machine (Struers, Copenhagen, Denmark). The electrolyzation solution was a mixed liquid of 30% nitric acid and 70% carbinol, with the double spraying temperature being −35 °C to −25 °C, and the voltage being 15 V.

3. Results and Discussion

3.1. Mechanical Properties

Table 1 lists the normal temperature tensile performance data of 2524 aluminum alloy under the three treatment states of T3, AA, and CA, and Figure 1 presents the fatigue life data of alloy under the three states.

Table 1. Static tensile properties of examined alloy.

Sample	Tensile Strength/MPa	Yield Strength/MPa	Elongation/%
T3	477.65	339.72	18.53
AA	490.22	439.39	8.25
CA	503.17	462.17	8.56

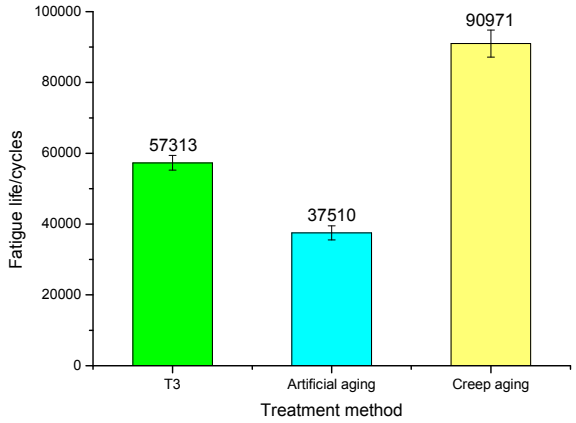

Figure 1. Fatigue lives of samples.

From Table 1, it can be seen that the strength of the alloys treated by artificial aging and creep aging enjoys a significant improvement over that of the alloy of the T3 state, with the tensile strength increasing by 5.5% and the yield strength increasing by 36%. Moreover, the strength of the alloy treated by creep aging is higher than that of the alloy treated by artificial aging, while the elongation of the alloys treated by artificial aging and creep aging is lower than that of the alloy of the T3 state.

From Figure 1, it can be seen that there are obvious differences among the three sample groups in terms of fatigue life. Fatigue life of the samples after creep aging treatment improves to the cycle number of 90971, almost 2 times more than the T3 alloy; and the fatigue life of the samples after artificial aging treatment decreased by the cycle number of about 20,000 when compared with T3 alloy.

3.2. Fatigue Fracture Analysis

Figure 2 presents the overall morphology of the fatigue fractures of the aluminum alloy at different states. It can be seen that all their macro fractures are similar, which can be divided into three areas, namely, fatigue source area, fatigue crack expansion area, and instant fracture area. Fatigue crack source area is located at the corner in a semi-circle; the following is a fatigue crack expansion area in the pattern of beach waves, where different interval arches and radial lines with the source area as the center can be observed; the morphology of the instant fracture area is similar to the regular tensile crack. Through comparing Figure 2a–c, it can be seen that the fatigue source area and the fatigue crack expansion area of the CA samples are the largest, followed by those of the T3 state. Those of the AA samples are the smallest. Given that the process of fatigue is a process of crack production and expansion, it can be concluded that the fatigue life of the CA samples is the best, followed by the T3 state and the AA samples successively, which is consistent with the test results of fatigue life.

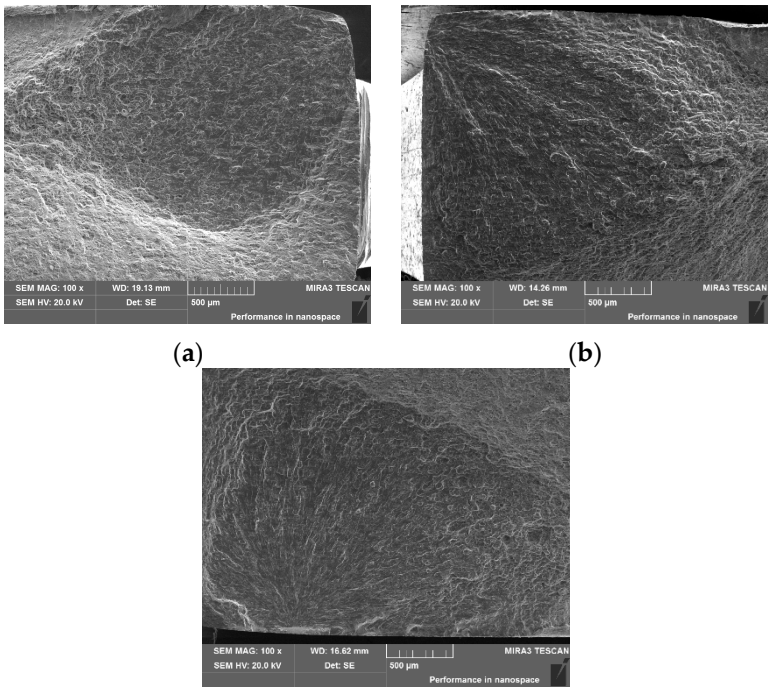

(**a**) (**b**)

(**c**)

Figure 2. The overall morphology of the fatigue fractures: (**a**) T3; (**b**) AA; (**c**) CA.

Figure 3 presents the SEM images after enlarging fatigue source area of three kinds of samples. It can be seen that the three kinds of samples are very similar, revealing cleavage-like feather-shaped morphology. Meanwhile, in some places, there are pits left by falling of rough second-phase particles where cracks concentrate.

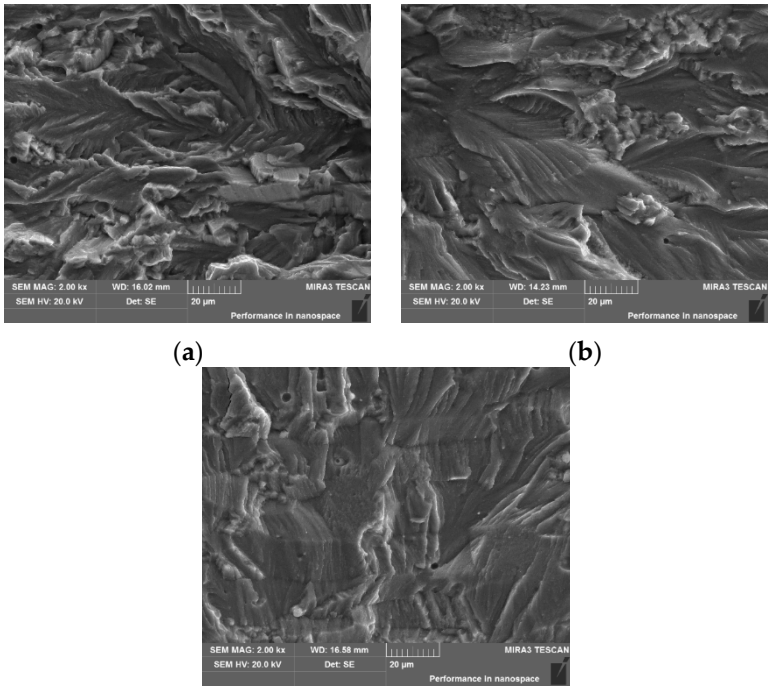

(**a**) (**b**)

(**c**)

Figure 3. Fatigue source area: (**a**) T3; (**b**) AA; (**c**) CA.

Figure 4 presents the SEM images after enlarging the fatigue crack expansion area of three kinds of samples. It can be seen that they all display obvious fatigue striation, which are micro traces left by crack expansion. Each belt can be regarded as an expansion trace of one instance of stress circle [14]. By comparing the distance among three sets of fatigue striation, it can be seen that, within the distance of 2 μm, there are about 11 fatigue striation on the T3 samples, 8 on the AA samples, and 15 on the CA samples. Besides, micro cracks can also be found on the fatigue striation of the AA samples, which shows that CA samples enjoy higher fatigue life followed by T3 samples, and AA samples have the lowest fatigue life.

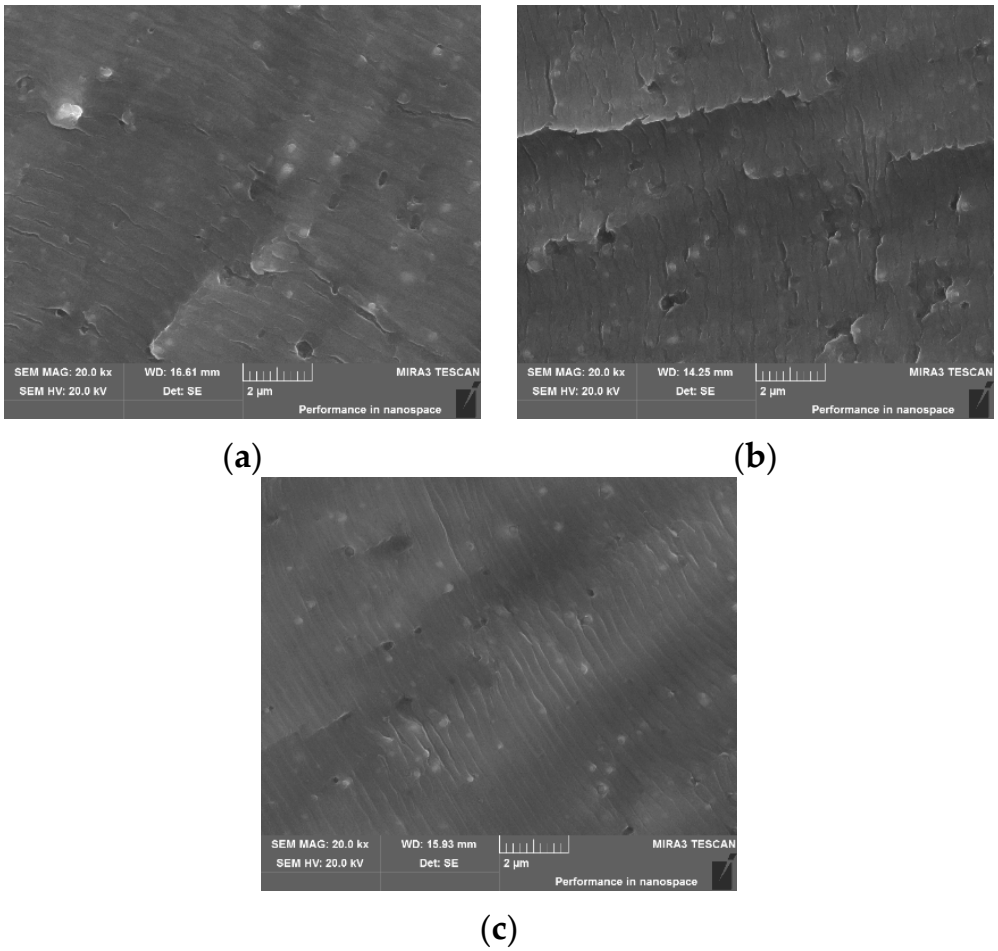

Figure 4. Fatigue crack expansion area: (**a**) T3; (**b**) AA; (**c**) CA.

Figure 5 presents the SEM images after enlarging the instant fracture area of the three kinds of samples. The three kinds of samples are similar, all showing morphology similar to the fracture at the normal-temperature static tensile test, and most of the parts on the fracture surface are dimples.

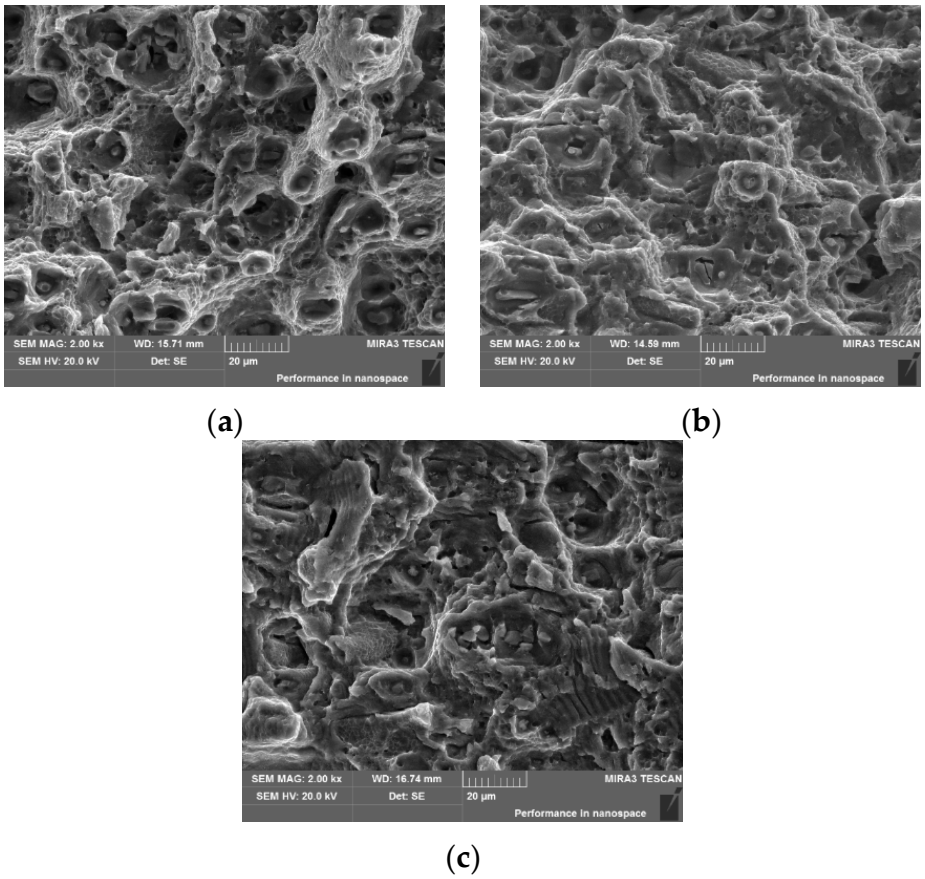

Figure 5. Instant fracture area: (**a**) T3; (**b**) AA; (**c**) CA.

3.3. Microstructure

Figure 6 presents the TEM micro structure of the 2524 aluminum alloy under the three states of T3, artificial aging, and creep aging. It can be discovered that there is no precipitated phase in the 2524-T3 aluminum alloy, showing that the enhanced phase mainly concentrates on the GPB area. Meanwhile, there are many baton-shaped T phases in the alloy crystal, results of the incomplete dissolution of solid solution [15]. There are needle-shaped S phases and S precipitated phases in the CA and AA samples, and these precipitations are not large, which can pin the dislocations. Therefore, the strength of the AA and CA samples is higher than that of the T3 samples. By comparing CA and AA samples, it can be seen that the precipitated phases in the CA samples slightly outnumber those in the AA samples, mainly because the CA samples are treated by creep aging, in which the presence of stress triggers partial plastic deformation in the substrate of the alloy, hence increasing the dislocation density, offering more space for second-phase core and facilitating the precipitation of a transgranular second phase. Figure 6 presents the TEM images of the crystal boundary of the samples in the three states. Phases precipitated at the crystal boundary of the T3 samples are continuously distributed, where even some T phases occur. However, there are already changes to precipitated phases at the boundary of the AA and CA samples, because the precipitated phase precipitation, combination, and aggregation at the crystal boundary of samples lead to the discontinuous distribution of the precipitated phases at the crystal boundary. Meanwhile, there is also a precipitation-free zone at a width of about 60 nm at the crystal boundary of the CA samples, but this cannot be found in the AA samples. The reason lies in the fact that, without stress, there is a huge difference in energy between the crystal boundary and inside the crystal boundary. After the introduction of stress, the energy difference drops, which leads to even precipitation momentum inside the boundary and at the crystal boundary; hence, no precipitation-free zone at the crystal boundary of the CA samples is narrow or even absent.

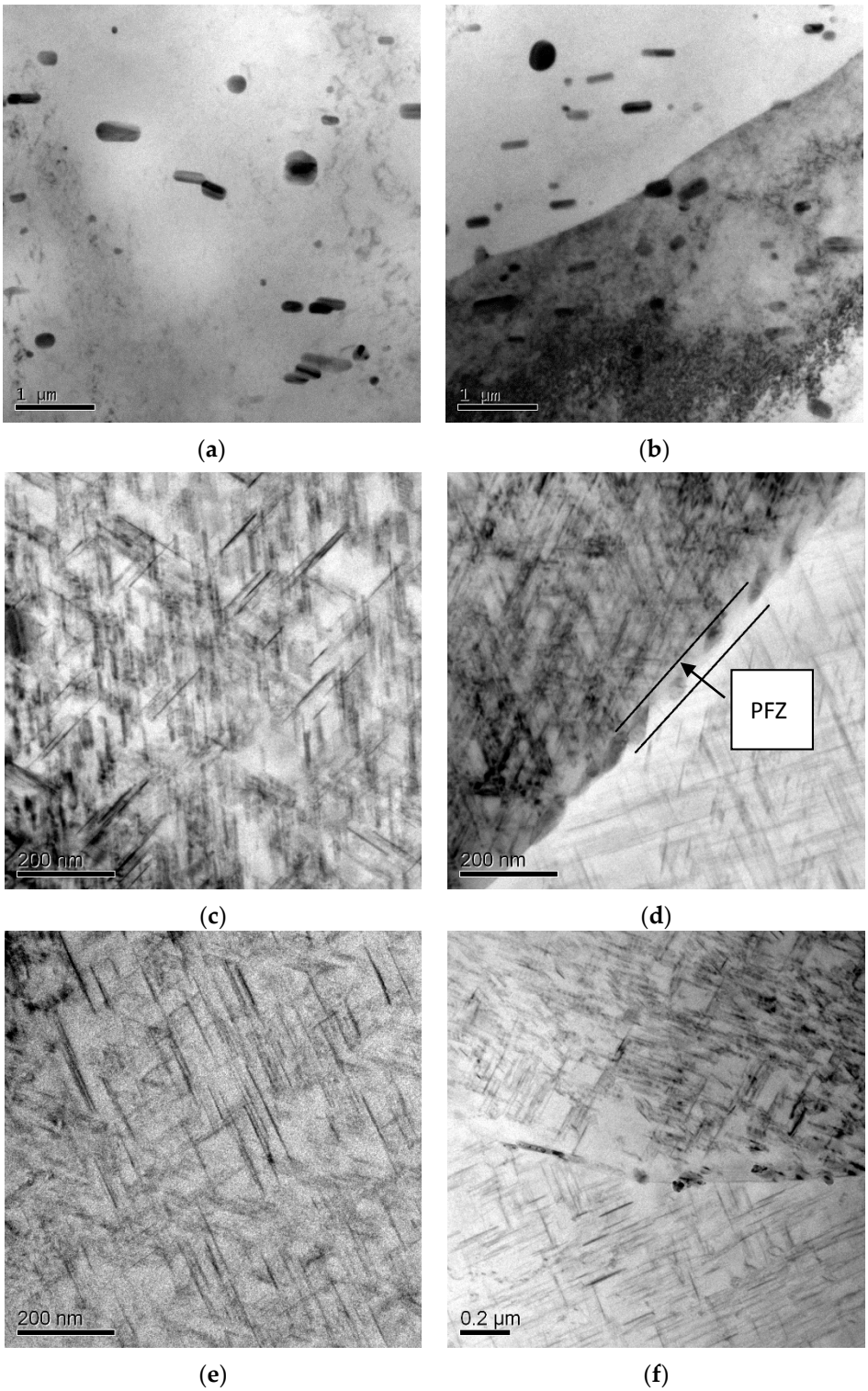

Figure 6. Aging precipitation characteristics of samples: (**a**,**b**) T3; (**c**,**d**) AA; (**e**,**f**) CA.

3.4. Discussion

The fatigue process of an alloy is the process of crack production and expansion, so fatigue life is the sum of the fatigue cycle number of crack production, crack expansion, and instant fracture. In this research, all the initial states of the alloys are T3, so the major difference among them lies in the aging stage after solid solution. Due to a low aging temperature, no great impact will be exerted upon

crystal particle structure or the rough second phase of the alloy, so the major influence of alloy fatigue performance lies in the aging precipitation features under different states.

For the Al-Cu-Mg alloy, its desolvation phase in the aging process is mainly θ phase and S phase, which turn out to be a competitive precipitation process. From the Al-Cu-Mg ternary phase diagram and relevant literature [16], when the mass fraction ratio between Cu and Mg reaches 1.5–4, S phase will be the main enhanced phase of the alloy. The Cu/Mg ratio of the 2524 aluminum alloy is about 3.13, so the precipitation sequence at 180 °C is GPB–S″–S′–S [17].

The influence of aging precipitation features upon alloy fatigue performance is mainly displayed in three aspects. Firstly, the presence of inside crystal precipitated phase can increase the strength of the alloy and enhance its anti-plastic deformation ability, so as to reduce its deformation damage. Secondly, the precipitated phase is semi-coherent or non-coherent with the base body, which leads to the dislocation in the fatigue process when going through the precipitated phase, leaving behind dislocation rings and thus increasing the resistance of reverse slipping of dislocation when loading decreases and disabling dislocation to slip repeatedly within the crystal. Meanwhile, the presence of precipitation-free zone (PFZ) decreases the strength of the crystal boundary, enabling the dislocation to slip at the boundary and increasing the stress concentration upon it. Therefore, the alloy is more likely to crack along the crystal boundary.

The GPB in the crystal of the T3 alloy is coherent with aluminum substrate, and it only has a common effect upon the enhancement of the base body, so its ability of anti-plastic deformation is not remarkable. However, in fatigue deformation, slipping dislocation can cut these GPB areas, causing minor fatigue damages. Meanwhile, there are no rough precipitated phases or PFZ at the crystal boundary of the T3 alloy, so the strength between the crystal boundary and inside the crystal is the same, without causing dislocation to slip at the boundary. There are many S′ phases inside crystal of the AA samples that fixed the dislocation, increasing its strength and the anti-plastic deformation ability. However, these precipitated phases are semi-coherent or non-coherent with the base body, the dislocation in the fatigue process going through the precipitated phase and leaving behind dislocation rings, so the deformation damage is big. There is about 60-nm PFZ at the crystal boundary of the AA samples and the precipitated phases are rough, decreasing the combination degree between the crystal particles and ultimately inviting fatigue crack. The transgranular precipitated phases of CA samples outnumber those of the AA samples, so the mechanical performance of CA samples is higher than that of the AA samples; and the anti-plastic deformation ability of the CA samples is increased as well. Meanwhile, due to the narrowness or absence of PFZ at the crystal boundary for the existence of stress, its morphology of the CA samples is similar to T3 samples, and the strength between the crystal boundary and inside the crystal is the same, so dislocation will not slip at the boundary.

Based on the above, the CA samples enjoy the highest fatigue life followed by the T3 state, and the AA samples are the lowest.

4. Conclusions

(1) Mechanical performance of samples after artificial aging and creep aging has enjoyed significant improvement over that of the T3 alloy. Fatigue life of the alloy through creep aging has also enjoyed improvement over that of the T3 alloy, and the fatigue life of samples after artificial aging treatment drops.

(2) The fatigue fracture morphology of samples in three states is divided into the fatigue source area, the fatigue crack expansion area, and the instant fracture area. Among them, the morphological difference of the fatigue crack expansion area is the largest, fatigue striation of the creep aging alloy is relatively narrow, and there are micro cracks appearing at the fatigue striation of the artificial aging alloy.

(3) All samples treated by artificial aging and creep aging precipitate S′ phases, about 60-nm PFZ appears at the crystal boundary of the samples treated by artificial aging, and the PFZ of the samples treated by creep aging is narrow or even absent.

(4) Transgranular phase precipitation can improve the anti-plastic deformation ability of materials, hence raising the fatigue life of alloy. The presence of rough second phases and PFZ at the crystal boundary is likely to make the alloy crack at the boundary, lowering its fatigue life.

Acknowledgments: This work was supported by the Fundamental Research Funds for the Central Universities of Central South University (No. 2016zzts318), the Key Program of the National Science Foundation of China (No. 51235010) and the National Key Basic Research Development Pan Funded Project of China (No. 2014cb046602).

Author Contributions: Wenke Li and Lihua Zhan conceived and designed the experiment; Lingfeng Liu and Wenke Li performed the experiments; Wenke Li and Yongqian Xu analyzed the data; Lingfeng Liu contributed reagents, materials and analysis tools; Wenke Li wrote the paper.

Conflicts of Interest: The authors declare no conflicts of interest.

References

1. Zeng, Y.; Huang, X. Forming Technologies of Large Integral Panel. *Acta Aeronaut. ET Astronaut. Sin.* **2008**, *3*, 721–727.
2. Zhan, L.; Lin, J.; Dean, T.A. A review of the development of creep age forming: Experimentation, modelling and applications. *Int. J. Mach. Tools Manuf.* **2011**, *51*, 1–17. [CrossRef]
3. Holman, M.C. Autoclave age forming large aluminum aircraft panels. *J. Mech. Work. Technol.* **1989**, *20*, 477–488. [CrossRef]
4. Levers, A.; Prior, A. Finite element analysis of shot peening. *J. Mater. Process. Technol.* **1998**, *80–81*, 304–308. [CrossRef]
5. Zhan, L.; Lin, J.; Dean, T.A.; Huang, M. Experimental studies and constitutive modelling of the hardening of aluminium alloy 7055 under creep age forming conditions. *Int. J. Mech. Sci.* **2011**, *53*, 595–605. [CrossRef]
6. Hargarter, H.; Lyttle, M.T.; Starke, E.A. Effects of preferentially aligned precipitates on plastic anisotropy in Al-Cu-Mg-Ag and Al-Cu alloys. *Mater. Sci. Eng. A* **1998**, *257*, 87–99. [CrossRef]
7. Zhan, L.; Li, Y.; Huang, M. Microstructures and properties of 2124 alloy creep ageing under stress. *J. Cent. South Univ. Sci. Technol.* **2012**, *3*, 926–931.
8. Chen, Y.; Deng, Y.; Wan, L.; Jin, K.; Xiao, Z. Microstructure and Properties of 7050 Aluminum Alloy Sheet During creep Aging. *J. Mater. Eng.* **2012**, *1*, 71–76.
9. Zabett, A.; Plumtree, A. Microstructural effects on the small fatigue crack behavior of an aluminum alloy plate. *Fatigue Fract. Eng. Mater. Struct.* **1995**, *18*, 801–809. [CrossRef]
10. Carter, R.D.; Lee, E.W.; Starke, E.A.; Beevers, C.J. The effect of microstructure and environment on fatigue crack closure of 7475 aluminum alloy. *Metall. Mater. Trans. A* **1984**, *15*, 555–563. [CrossRef]
11. Bray, G.H.; Glazov, M.; Rioj, R.J.; Lib, D.; Gangloffb, R.P. Effect of artificial aging on the fatigue crack propagation resistance of 2000 series aluminum alloys. *Int. J. Fatigue* **2001**, *23*, 265–276. [CrossRef]
12. Williams, J.C.; Starke, E.A. Jr. Progress in structural materials for aerospace systems. *Acta Mater.* **2003**, *51*, 5775–5799. [CrossRef]
13. Chen, W. Application of advanced aluminum alloys in A380 structures. *Aviat. Maint. Eng.* **2005**, *2*, 40–41.
14. Shu, D. *Mechanical Properties of Engineering Materials*, 1st ed.; Machinery Industry Press: Beijing, China, 2007.
15. Cheng, S.; Zhao, Y.H.; Zhu, Y.T.; Ma, E. Optimizing the strength and ductility of fine structured 2024 Al alloy by nano-precipitation. *Acta Mater.* **2007**, *55*, 5822–5832. [CrossRef]
16. Liu, Z.; Li, Y.; Liu, Y.; Xia, Q. Development of Al-Cu-Mg-Ag alloys. Chin. *J. Nonferr. Met.* **2007**, *12*, 1905–1915.
17. Wang, S.C.; Starink, M.J. Precipitates and intermetallic phases in precipitation hardening Al-Cu-Mg-(Li) based alloys. *Int. Mater. Rev.* **2013**, *50*, 193–215. [CrossRef]